Hypoxia and Wnt signaling inversely regulate expression of chondroprotective molecule ANP32A in articular cartilage

Jolien Quintiens[1,2], Astrid De Roover[1], Frederique M. F. Cornelis[1], Ana Escribano-Núñez[1], An Sermon[3,4], Sofia Pazmino[5], Silvia Monteagudo[1†], Rik J. Lories[1,2*†]

[1] Laboratory of Tissue Homeostasis and Disease, Skeletal Biology and Engineering Research Center, Department of Development and Regeneration, KU Leuven, Leuven, Belgium.
[2] Department of Rheumatology, University Hospitals Leuven, Leuven, Belgium.
[3] Department of Trauma Surgery, University Hospitals Leuven, Leuven, Belgium.
[4] Trauma Research and Innovation Center, Department of Development and Regeneration, KU Leuven, Leuven, Belgium.
[5] Clinical Research Unit, Skeletal Biology and Engineering Research Center, KU Leuven, Department of Development and Regeneration, KU Leuven, Leuven, Belgium.

[†] S. Monteagudo and R.J Lories equally contributed as senior and corresponding authors.
* Address correspondence and reprint requests to: Prof. R. Lories or Prof. S. Monteagudo, Skeletal Biology and Engineering Research Center, Herestraat 49 Box 813, B-3000, Leuven, Belgium – 32-16-342541; Fax: +32-16-342543; Email: Rik.Lories@kuleuven.be – Silvia.Monteagudo@kuleuven.be

E-mail addresses:
jolien.quintiens@kuleuven.be; astrid.deroover@kuleuven.be; frederique.cornelis@kuleuven.be; anaescribano.escribanonunez@kuleuven.be; an.sermon@kuleuven.be; sofia.pazmino@kuleuven.be; silvia.monteagudo@kuleuven.be; rik.lories@kuleuven.be

Abstract

Objectives: ANP32A is a key protector of cartilage health, via preventing oxidative stress and Wnt hyper-activation. We aimed to unravel how *ANP32A* is regulated in cartilage.

Methods: A bioinformatics pipeline was applied to identify regulators of *ANP32A*. Pathways of interest were targeted to study their impact on ANP32A in *in vitro* cultures of the human chondrocyte C28/I2 cell-line and primary human articular chondrocytes (hACs) from up to 5 different donors, using Wnt-activator CHIR99021, hypoxia-mimetic IOX2 and a hypoxia chamber. ANP32A was evaluated using RT-qPCR and Western blot. *In vivo*, the effect of hypoxia was examined by immunohistochemistry in mice injected intra-articularly with IOX2 after destabilization of the medial meniscus. Effects of Wnt hyper-activation were investigated using *Frzb*-knockout mice and wild-type mice treated intra-articularly with CHIR99021. Wnt inhibition effects were assessed upon intra-articular injection of XAV939.

Results: The hypoxia and Wnt signaling pathways were identified as networks controlling ANP32A expression. *In vitro* and *in vivo* experiments demonstrated increases in ANP32A upon hypoxic conditions (1.3-fold in hypoxia in C28/I2 cells with 95% confidence interval (CI) [1.11-1.54] and 1.90-fold in hACs [95%CI:1.56-2] and 1.67-fold in ANP32A protein levels after DMM surgery with IOX2 injections [95%CI:1.33-2.08]). Wnt hyper-activation decreased ANP32A in chondrocytes *in vitro* (1.23-fold decrease [95%CI:1.02-1.49]) and in mice (1.45-fold decrease after CHIR99021 injection [95%CI:1.22-1.72] and 1.41-fold decrease in *Frzb*-knockout mice [95%CI:1.00-1.96]). Hypoxia and Wnt modulated *ATM*, an ANP32A target gene, in hACs (1.89-fold increase [95%CI:1.38-2.60] and 1.41-fold decrease [95%CI:1.02-1.96]).

Conclusions: Maintaining hypoxia and limiting Wnt activation sustain *ANP32A* and protect against osteoarthritis.

Keywords: ANP32A, Wnt signaling, Hypoxia, Articular cartilage

Running title: Hypoxia and Wnt signaling regulate ANP32A

Introduction

Maintaining cartilage homeostasis is key to prevent onset and progression of osteoarthritis (OA). In OA, articular chondrocytes die or lose their specific molecular features, resulting in a biomechanically inferior extracellular matrix and suboptimal joint lubrication. The mechanisms that control the molecular identity of the articular chondrocyte remain incompletely understood, precluding the development of effective treatments for OA. Acidic leucine-rich nuclear phosphoprotein-32A (ANP32A), a multifunctional ubiquitously expressed intracellular protein, was earlier genetically associated with OA[1-5]. Then, we demonstrated that *Anp32a*-knockout mice exhibit more severe cartilage damage in different mouse models of the disease, as compared to wild-type mice[1]. ANP32A is a key protective molecule in OA that limits excessive oxidative stress via enhancing the expression of the ataxia-telangiectasia mutated serine/threonine kinase (*ATM*) gene[1]. ANP32A is also able to restrict excessive activation of Wnt signaling, a cascade that when hyper-activated contributes to joint disease[3, 6, 7].

Levels of *ANP32A* are reduced in the articular cartilage of patients with OA compared to non-OA tissue[1]. Thus, maintaining *ANP32A* levels seems crucial to safeguard cartilage health and a strategy for therapy in OA. However, the factors that regulate expression of *ANP32A* in the articular chondrocyte remain unknown.

Bioinformatic tools allow *in silico* interrogation of the regulation of a gene of interest. We developed and validated a pipeline that can be applied to gene expression studies in the articular chondrocyte[8]. Here, we identified factors that regulate *ANP32A*, and then performed functional studies to gain insights into the effects of identified regulatory networks, namely hypoxia and Wnt signaling.

83

Materials and Methods

Patient materials. Primary human articular chondrocytes (hACs) were isolated from patients undergoing hip replacement surgery for osteoporotic or malignancy-associated fractures with informed consent and ethical approval by the University Hospitals Leuven Ethics Committee. Under Belgian Law and UZ Leuven's biobank policies, the joints are considered biological residual material. Only age and sex are being shared between surgeons and investigators (Supplementary table 1). The hips were macroscopically evaluated to exclude OA.

Bioinformatics analysis. The bioinformatics analysis was conducted as described[8]. Briefly, four online tools, ConSite (http://consite.genereg.net)[9], TFsitescan (http://www.ifti.org/Tfsitescan)[10], BindDB (http://bind-db.huji.ac.il)[11], and PROMO (http://alggen.lsi.upc.es)[12], were interrogated for factors predicted to interact with the *ANP32A* proximal promoter sequence (1000 basepairs upstream and 100 basepairs downstream relative to the transcription start site), obtained from the online Eukaryotic Promoter Database (EPD) tool (https://epd.epfl.ch)[13](Supplementary table 2A). ConSite, PROMO and TFsitescan align the promoter DNA sequence and calculate potential transcription factor (TF) binding based on TF position weight matrix (PWM)[9, 12, 14, 15]. They use the following PWM databases respectively: JASPAR, TRANSFAC and the relational Transcription Factors Database[9, 10, 12]. BindDB not only provides information on TFs, but also on epigenetic data (e.g. histone modifications). It uses ChIP-seq data performed by the Meshorer Lab, and data from ENCODE, Roadmap and the GEO repository[11]. Outputs from the four different tools were compared and only TFs predicted by at least 2 different tools were selected for further analysis. Potential specificity for *ANP32A* was interrogated *in silico* by assessing binding of these TFs to the promoters of aggrecan, collagen 2a1 and actin. STRING (https://string-db.org)[16], HumanBase

(https://hb.flatironinstitute.org)[17] and Ingenuity pathway analysis (IPA)[18] were used to explore protein-protein interactions and cartilage-specific regulatory networks of the predicted TFs (Supplementary table 2B), respectively.

Cell culture. Human immortalized differentiated chondrocyte C28/I2 cells[19] were purchased from Merck Millipore. For the isolation of hACs, samples were processed as described[8]. Chondrocytes were cultured in DMEM/F12 (Gibco) containing 10% fetal bovine serum (Gibco), 1% (vol/vol) antibiotic/antimycotic (Gibco) and 1% L-glutamine (Gibco) in a humidified atmosphere at 37°C and 5% CO_2.

Quantitative PCR. Total RNA was extracted using the Nucleospin RNA II kit (Macherey-Nagel). cDNA was synthesized using the RevertAidHminus First Strand cDNA synthesis kit (Thermo Fisher Scientific). Quantitative PCR analyses were carried out as described using Maxima SYBRgreen qPCR master mix system (Thermo Fisher Scientific)[20]. Gene expression was calculated following normalization to housekeeping gene 29S using the comparative Ct (cycle threshold) method. The following PCR conditions were used: incubation for 10 min at 95°C followed by 40 amplification cycles of 15 s of denaturation at 95°C followed by 45 s of annealing-elongation at 60°C. Melting curve analysis was performed to determine specificity. Primers are listed in Supplementary Table 3.

Cell lysis and Western blotting. Cells were lysed in IP Lysis/Wash buffer (Thermo Fisher) supplemented with 5% (vol/vol) Protease Mixture Inhibitor (Sigma), 1 mM phenylmethanesulfonyl (Sigma), 5 mM sodium fluoride (Sigma) and 2.3 mM sodium orthovanadate (Sigma). After one homogenization cycle (7 s) with an ultrasonic cell disruptor (Microson; Misonix), total cell lysates were centrifuged at 18,000 g for 10 min. The supernatant

was collected and the protein concentration was determined by Pierce BCA Protein Assay Kit (Thermo Scientific). Immunoblotting analysis was carried out as described[20]. Antibodies used were against Actin (Sigma, A2066; dilution 1:4,000), ANP32A (Abcam, ab189110, dilution 1:1,000) and hypoxia-inducible factor-1 α (HIF1A) (Abcam, ab82832; dilution 1:1,000). The blotting signals were detected using the SuperSignalWest Femto Maximum Sensitivity Substrate system (Thermo Scientific).

ChIP analysis. Chromatin immunoprecipitation (ChIP) assays were performed as described, using the Agarose ChIP kit (Thermo Fisher Scientific)[3, 8]. Cell samples were cross-linked with 1% formaldehyde for 10 min and glycine added to a 125 mM final concentration. Fixed cells were lysed and chromatin was fragmented by nuclease digestion. Further, the sheared chromatin was incubated with antibodies against HIF1A (Abcam, ab1; dilution 1:50) and HIF2A (Abcam, ab199; dilution 1:50) and recovered by binding to protein A/G agarose. Eluted DNA fragments were used for qPCR.

Pharmacological compounds. IOX2, CHIR99021 (CHIR) and XAV939 (XAV) were purchased from MilliporeSigma, Sigma-Aldrich and Selleck Chemicals.

Mouse models. Animal experiments are reported following the ARRIVE guidelines (https://www.nc3rs.org.uk/arrive-guidelines) (Supplementary Table 4 and ARRIVE checklist). All studies were approved by the Ethics Committee for Animal Research (P159-2016, P004-2022; KU Leuven, Belgium) (License LA1210189). Wild-type male C57Bl/6J mice, used as controls and for intra-articular injections, were purchased from Janvier (Le Genest St Isle, France). Mice were not specifically randomized, but assigned to the group by the investigator at the time of labelling.

In male C57Bl/6J wild-type mice, 8 weeks of age, post-traumatic OA was induced by destabilization of the medial meniscus (DMM) surgery[21]. Sham-surgery served as control. One week after DMM surgery, mice were intra-articularly injected with IOX2 (0.5 mg/kg) or vehicle (30% PEG400 in PBS) every 10 days for a total of 7 injections. 12 weeks after surgery, the knees were harvested and analyzed.

Eight week-old wild-type male C57Bl/6J mice were treated with an intra-articular injection of CHIR 1 mg/kg or vehicle (6% DMSO, 40% PEG400 in PBS) on day 1 and day 4. The knees were harvested at 9 weeks of age.

Frizzled-related protein knockout (*Frzb*$^{-/-}$) mice were backcrossed onto the C57Bl/6J background for more than 20 generations[22]. Wild-type littermates were used as control. *Frzb*$^{-/-}$ male mice were harvested untreated at 8 weeks of age.

Eight week-old wild-type male C57Bl/6J mice were treated with an intra-articular injection of XAV 0.5 mg/kg or vehicle (ethanol) twice a week for 2 weeks. The knees were harvested at 12 weeks of age.

Histology. Dissected mouse knees were fixed overnight at 4°C in 2% formaldehyde, decalcified for 3 weeks in 0.5M EDTA pH 7.5, and embedded in paraffin. All stainings were performed on 5 µm thick sections. Pictures were taken using a Visitron Systems microscope (Leica Microsystems).

Immunohistochemistry. Heat-induced epitope retrieval was performed using Citrate-EDTA buffer (pH 6.2, for TCF1) or Na-citrate buffer (0.5 M, pH 6.0, for ANP32A and HIF1A) for 10 min at 95°C. Sections were treated with 3% H_2O_2/methanol for 10 min to inactivate endogenous peroxidase, blocked in goat serum for 30 min and incubated overnight at 4°C with primary antibodies against ANP32A (Abcam, ab189110, 10 µg/ml), HIF1A (Abcam, ab82832, 10 µg/ml) or TCF1 (Ab96777, Abcam; 10 µg/ml). Rabbit IgG (Santa Cruz, sc-2027) was used as negative control. Avidin-biotin complex amplification (Vectastain ABC kit, Vector Laboratories) was used. Peroxidase goat anti-rabbit IgG (Jackson Immunoresearch) was applied for 30 min and peroxidase activity determined using 3,3'-diaminobenzidine (DAB). Quantification of immunohistochemical staining was performed with 'Colour Deconvolution plugin' (Jacqui Ross, Auckland University) in ImageJ Software (NIH Image, National Institutes of Health Bethesda, Maryland, USA)[23, 24]. The software deconvolutes images according to a DAB staining-specific protocol, isolating the brown color (DAB) and the blue color (Haematoxylin) in 2 separate images. This image is then converted to black-and-white and the intensity of the black area is measured. To minimize variability, we used the same threshold for each isolated color in every experiment. Quantification was performed using two technical replicates for 3-5 different samples, with staining intensity reported relative to the average of control mice in the experiment.

Statistical analysis. Data analysis and graphical presentation were performed with GraphPad Prism version 9.3.1. The *in vitro* and *ex vivo* analyses were considered exploratory and no formal power calculation was made. Data are presented as mean and standard deviation (SD) or individual data points, representing the mean of technical replicates as indicated in figure legends. Data analysis assumptions were tested by visual inspection of distribution, by QQ-,

homoscedasticity and residuals plots. Gene expression data and image quantifications were log-transformed for statistical analysis.

For experiments with hACs, each donor was considered as an independent biological replicate. Different treatments within one donor sample were considered non-independent (paired). All tests were two-tailed. For comparisons between 2 groups, unpaired 2-tailed Student's t-test was performed (two condition gene expression studies in C28/I2 cells, two condition immunohistochemistry experiments). For comparisons between 2 groups with non-independent data, paired 2-tailed Student's t-test was used (two condition gene expression studies in hACs). For comparisons between more than 2 groups, one-way ANOVA was used, with Dunnett correction for multiple comparisons (multi-dose gene expression studies in C28/I2 cells and multifactor analysis of immunohistochemistry studies). For comparisons against a hypothetical mean (1) in the ChIP experiments, one-sample, 2-tailed t-test was used. Data are reported by effect sizes, confidence intervals (CI) and the *p*-values. *P*-values equal to or less than 0.05 were considered significant.

Results

Identification of ANP32A regulating factors by bioinformatics

To identify molecules that regulate expression of *ANP32A*, we applied a bioinformatics pipeline (Figure 1A). The sequence of the human *ANP32A* gene promoter was obtained using the EPD tool[13](Supplementary Table 2A). Four bioinformatic tools were interrogated for regulatory factors predicted to interact with the *ANP32A* promoter[9-12]. This resulted in 209 hits, mostly TFs. We then selected regulatory factors simultaneously predicted by at least two databases, resulting in 49 TFs (Figure 1A, B and Supplementary Table 2B). Next, a specificity analysis was performed to identify TFs that might be more selective for *ANP32A*. To this end, TFs that were also predicted to regulate genes that characterize the chondrocyte identity (aggrecan and collagen type 2a), as well as the housekeeping gene actin, were excluded by two approaches. In the first, the EPD Search Motif tool was used to determine whether a predicted TF could also bind to the promoter of the three mentioned control genes (Figure 1A, C)[13]. In the second approach, the promoter sequences of the three control genes were analyzed using the same bioinformatic tools as for *ANP32A*, and we determined whether any of the selected TFs appeared in the output (Figure 1A, C). Combining both approaches resulted in a shortened list of 16 TFs (Figure 1A, C and Supplementary Table 2C).

Network analysis suggests hypoxia and Wnt signaling pathways as regulators of ANP32A expression

To explore interaction networks built from the resulting TFs identified in the bioinformatics analysis, we performed network analysis using the HumanBase tool[17] (Figure 2A), which

allows to build cartilage-specific networks, and the STRING database[16] (Figure 2B), which integrates known and predicted protein-protein interactions. We also performed pathway enrichment analysis using IPA software[18] (Figure 2C). The network building algorithm from HumanBase pointed out a network linked to hypoxia as one of five major cartilage-specific modules that regulate *ANP32A* expression based on the combination of the 49 TFs and known tissue-specific expression profiles (Figure 2A, Supplementary Table 2D). Under physiological conditions, articular cartilage is hypoxic. Loss of its hypoxic nature is associated with OA, and restoring hypoxia is beneficial for the disease[8, 25, 26]. Hypoxia Inducible Factors (HIFs) are heterodimers, composed of an oxygen-sensitive α-subunit and a β-subunit, which bind to hypoxia response elements (HREs) in the genome to induce a transcriptional response[27, 28]. We identified an HRE with consensus sequence 5'-(A/G)CGTG-3' in the *ANP32A* promoter (Figure 2D)[28, 29].

Among signaling pathways identified by STRING (Figure 2B) and IPA (Figure 2C), we encountered Wnt/beta-catenin signaling, a cascade strongly linked to OA and proven to be detrimental for cartilage health when hyper-activated[7, 30-32]. TCF/LEF factors are TFs that ultimately mediate the transcriptional response to Wnt signaling. TCF/LEF were found among the 16 final hits obtained after applying the specificity analysis (Figure 1C and Supplementary Table 2C). We identified two Wnt response elements (WRE) for TCF/LEF in the *ANP32A* promoter[29, 33] (Figure 2E). These data suggest that the hypoxia and the Wnt signaling pathways regulate expression of *ANP32A* in the articular chondrocyte.

Hypoxia increases ANP32A expression in the articular chondrocyte

To investigate effects of hypoxia on *ANP32A* expression, we performed experiments in human chondrocytes using the pharmacological hypoxia mimetic IOX2 or a hypoxic cell culture environment (1% O_2). IOX2 is an inhibitor of prolyl hydroxylase-2 (PHD2), an enzyme that targets HIF1A for proteasomal degradation in normoxic conditions[25, 34]. In the C28/I2 cell line, treatment with IOX2 did not consistently increase *ANP32A* mRNA transcription levels (1.36-fold (95%CI[0.87-2.10], p=0.18) with 20 µM IOX2 and 1.33-fold (95%CI[0.85-2.06], p=0.21) with 50 µM IOX2) (Figure 3A). However, incubation of the C28/I2 chondrocytes in a hypoxia chamber increased *ANP32A* mRNA transcription levels 1.31-fold (95%CI[1.11-1.54], p=0.01) (Figure 3B). As expected, expression of Vascular Endothelial Growth Factor (*VEGF),* a hypoxia target gene used as positive control, increased by IOX2 treatment 3.12-fold with 20 µM IOX2 (95%CI[2.29-4.14], p<0.0001) and 5.25-fold with 50 µM IOX2 (95%CI[3.91-7.06], p<0.0001) and 3.08-fold in hypoxia culture (95%CI[2.35-4.03], p=0.0003) (Figure 3A, B). Then, we examined the effects of hypoxia on ANP32A at the protein level, using Western blot analysis. Both treatment with IOX2 and incubation in a hypoxia chamber increased protein amounts of ANP32A (Figure 3C, D). Next, we validated these data in hACs. Treatment with IOX2 and incubation in a hypoxia chamber increased *ANP32A* mRNA expression 1.32-fold (95%CI[1.14-1.52], p=0.01) and 1.90-fold (95%CI[1.56-2], p=0.0009) respectively (Figure 3E, F). *VEGF* expression was increased 8.37-fold (95%CI[4.90-14.32], p=0.0004) and 5.13-fold (95%CI[2.73-9.64], p=0.002) respectively. These data demonstrate that hypoxia increases *ANP32A* mRNA and protein levels in the human articular chondrocyte.

We next sought to determine whether hypoxia is able to increase *ANP32A* in OA and protect against disease. We induced OA by subjecting 8 week-old male wild-type C57Bl/6J mice to the DMM surgery[21]. After one week, we administered the hypoxia mimetic IOX2 via intra-articular injections every 10 days until mice were 20 weeks-old. After DMM surgery, amounts of

ANP32A (and of positive control HIF1A) were decreased 3.28-fold (95%CI[2.60-4.13], $p<0.0001$) as compared to sham-treated mice (Figure 3G and Figure S1). Treatment with IOX2 partially rescued ANP32A amounts after DMM surgery 1.67-fold (95%CI[1.33-2.08], $p=0.0002$) (Figure 3G and Figure S1). These data evidence the enhancing effect of hypoxia on *ANP32A* expression in cartilage in an OA mouse model.

Hypoxia induces ANP32A transcription via HIF1A

We investigated molecular mechanisms via which hypoxia increases *ANP32A* transcription. In mammals, there are three isoforms of the α-subunit: HIF1A, HIF2A and HIF3A[28]. Within human cartilage, HIF1A mainly promotes cartilage homeostasis and health, while HIF2A is associated with hypertrophic differentiation of chondrocytes and cartilage degradation[26, 35, 36]. Knowledge about HIF3A and its expression in cartilage is limited[37]. To investigate the underlying mechanism of *ANP32A* increase upon hypoxia, we performed ChIP-qPCR in C28/I2 chondrocytes treated with IOX2 and investigated binding of HIF1A and HIF2A to the *ANP32A* promoter. This analysis showed that HIF1A (2.72-fold (95%CI[1.54-4.80], $p=0.02$)) but not HIF2A (0.34-fold (95%CI[0.02-4.81], $p=0.22$)) binds to the *ANP32A* gene promoter (with binding of HIF1A to *VEGF* 2.68-fold (95%CI[1.08-6.67], $p=0.04$) and binding of HIF2A to *VEGF* 0.45-fold (95%CI[0.05-4.25], $p=0.26$)) (Figure 3H).

Hyper-activation of Wnt signaling decreases ANP32A expression in the articular chondrocyte

Next, we investigated effects of excessive Wnt signaling activation on *ANP32A* expression. hACs were treated with the pharmacological Wnt activator CHIR. CHIR is an inhibitor of

glycogen synthase kinase 3 beta (GSK3β), a component of the beta-catenin destruction complex[38]. Upon treatment with CHIR, *ANP32A* mRNA expression decreased 1.23-fold (95%CI[1.02-1.49], p=0.04). Expression of *TCF1*, a direct Wnt target gene used as positive control, was effectively enhanced 3.25-fold (95%CI[2.68-3.94], p<0.0001) (Figure 4A). This demonstrates that hyper-activation of Wnt signaling decreases *ANP32A* in hACs.

Next, we validated these findings *in vivo*, using different animal models. In the first, Wnt hyper-activation was induced by injecting CHIR intra-articularly in 8 week-old C57Bl/6J mice and confirmed by immunohistological staining for Wnt target gene TCF1. This led to a 1.45-fold decrease in ANP32A protein expression in articular cartilage (95%CI[1.22-1.72], p=0.0037), as examined with immunohistochemistry (Figure 4B) and to a 2.70-fold increase in TCF1 protein expression (95%CI[2.04-3.58], p=0.0006) (Figure S2A). Then, we used the *Frzb*-knockout mouse model, a Wnt gain-of-function genetic model since Frizzled-related protein (FRZB; also called secreted Frizzled-related protein 3 [sFRP-3]) is an extracellular antagonist in the Wnt signaling pathway[22]. In these mice, we also observed a decrease in ANP32A protein expression in articular cartilage compared to wild-type controls (1.41-fold decrease (95%CI[1.00-1.96], p=0.05)) and a 3.74-fold increase in TCF1 protein expression (95%CI[2.57-5.44], p =0.0006) (Figure 4C, Figure S2B). Finally, to investigate the translational implications of these findings, we investigated whether Wnt inhibition enhanced ANP32A expression in articular cartilage. We used XAV, a tankyrase inhibitor that stabilizes the β-catenin destruction complex[39]. We injected XAV intra-articularly in 8 week-old wild-type mice and observed an increase in ANP32A protein by 1.94-fold (95%CI[1.75-2.15], p<0.0001), as shown by immunohistochemistry and a 2.40-fold decrease in TCF1 protein expression (95%CI[0.31-0.55], p=0.001) (Figure 4D, Figure S2C). These results demonstrate that limiting Wnt signaling in articular cartilage boosts *ANP32A* expression.

346

347 **Hypoxia and Wnt signaling modulation impact the expression of antioxidant ATM**

348

349 Finally, we investigated whether modulation of hypoxia and Wnt signaling results in
350 downstream changes in *ATM* expression, a gene directly controlled by ANP32A, which encodes
351 a key effector in the prevention of oxidative stress[1, 40]. We observed increased expression of
352 *ATM* in hACs after IOX2 treatment (1.31-fold (95%CI[1.07-1.61], p=0.02)) (Figure 5A) and in
353 hACs incubated in a hypoxia chamber (1% O_2) (1.89-fold (95%CI[1.38-2.60], p=0.012))
354 (Figure 5B). Inversely, activation of Wnt signaling with CHIR resulted in decreased *ATM*
355 expression (1.41-fold (95%CI[1.02-1.96], p=0.04)) (Figure 5C). Hence, excessive Wnt
356 signaling negatively affects the *ANP32A-ATM* axis that protects the chondrocyte against
357 oxidative stress (Figure 5D).

358

Discussion

This study unravels two major regulatory pathways that control the expression of key cartilage protective molecule ANP32A. Hypoxia increases *ANP32A* expression in articular chondrocytes, while excessive activation of Wnt signaling negatively regulates *ANP32A* (Figure 5D). Our earlier work identified ANP32A as a key node in a complex network that sustains cartilage health[1, 3]. Hence, the unraveling of regulatory pathways that impact on *ANP32A* expression further identifies the maintenance of a hypoxic environment in articular cartilage, and inhibiting Wnt signaling hyper-activation as targets for therapeutic intervention in OA.

In addition, we corroborated the validity of our bioinformatics pipeline[8], showing that this approach can be applied for any gene of interest. When applied to find regulators of *ANP32A in silico*, we additionally identified other interesting pathways as potential regulators of *ANP32A* (Figure 2A, B, C). Among these are the senescence pathway and SUMOylation, both earlier associated with OA[41, 42]. These pathways and their role in OA provide further opportunities for research.

Under physiological and homeostatic conditions, articular cartilage is hypoxic but in OA, this hypoxic nature is lost[26, 36, 43]. Multiple studies have shown beneficial effects of restoring the joint hypoxic environment[26, 36, 44]. Our group demonstrated protective effects of restoring hypoxia on cartilage health in an OA model by intra-articular injections of IOX2[8]. Restoring hypoxia in articular cartilage led to an increase in the expression of *DOT1L*[8]. DOT1L is a histone methyltransferase key for cartilage health, and its function is decreased in OA, similarly

to ANP32A[20]. Here, we show that hypoxia enhances *ANP32A* expression *in vitro* and *in vivo* in the joints of mice subjected to DMM surgery.

Hyper-activation of Wnt signaling is a well-known culprit in OA. Physiological activation of this pathway is necessary for normal skeletal development and for adult joint homeostasis. However, Wnt hyper-activation is detrimental for cartilage[6, 31]. ANP32A limits Wnt signaling through an epigenetic mechanism as part of the inhibitor of histone acetyltransferase (INHAT) complex[3]. This indicates the existence of a negative feedback loop between ANP32A and Wnt signaling in articular cartilage, since they reciprocally limit each other[3]. Our data corroborate the complex orchestration of Wnt signaling, of which a meticulous balance between activation and inhibition is essential for cartilage health. Targeting this pathway is increasingly interesting in the treatment of OA[6, 30, 31]. A phase 2 clinical trial with Lorecivivint, a Wnt pathway modulator, showed a reduction in pain in a subgroup of patients with unilateral symptoms of knee OA after a single intra-articular injection[45]. A phase 3 clinical trial has been performed, but the results have yet to be disclosed (NCT03928184).

Here, we demonstrate that hypoxia has a direct regulatory effect on ANP32A since HIF1A interacts with the ANP32A promoter. However, indirect effects cannot be excluded, since it was previously reported that hypoxia and Wnt signaling interact[36]. Bouaziz et al. showed that HIF1A can inhibit Wnt signaling by blocking transcription factor 4 (TCF4)-β-catenin interaction[36]. This shows how these different pathways are intrinsically linked within a complex system that likely regulates articular cartilage homeostasis (Figure 5D).

Limitations of this work first include the use a human differentiated chondrocyte cell line that does not fully represent the molecular identity of a healthy articular chondrocyte. Yet, we validated these findings in primary human articular chondrocytes from donors without

osteoarthritis. These cells, available as waste material from other surgeries, are a relatively rare commodity for research, as cell expansion of chondrocytes leads to differentiation. Another limitation may be the non-agnostic approach to the pathway analysis in bioinformatics, thereby prioritizing mechanistic experiments in pathways already associated with chondrocyte biology and joint disease. Third, whereas the joint context suggests that the effects of HIF1A on ANP32A expression are mediated upstream by the hypoxic homeostatic environment of healthy articular cartilage, we cannot exclude the existence of hypoxia independent regulators of HIF1A. Of note, for our *in vitro* and *in vivo* experiments we report a number of positive controls using known target genes, namely VEGF and TCF1. Quantitative differences in expression levels between ANP32A and known target genes may result from different transcription factor activity or distinct post-translational mechanisms regulating gene expression. However, such different expression levels may not correlate with the magnitude of their biological effects. Finally, we provide evidence that hypoxia sustains and Wnt signaling represses ANP32A in the joint, but we did not address the specific contribution of increases in ANP32A in the IOX2 or XAV treated animals to reduce severity of OA. These interventions affect the activity of different pathways in the joint that are complex to entangle. The limited availability of *Anp32a*-deficient mice due to subfertility and the severe phenotype of these animals due to oxidative stress were factors considered not to perform additional animal experiments with this strain that we extensively characterized earlier[1, 3]. Future experiments will include exploring the oxidative stress level in chondrocytes upon ANP32A modulation and identifying the mechanisms via which Wnt regulates *ANP32A* expression.

In conclusion, we identified hypoxia and Wnt signaling as regulators of *ANP32A*. In combination with our previous work on ANP32A and DOT1L, we conclude that these two key

chondroprotective molecules are upregulated by hypoxia and prevent excessive Wnt signaling[3, 8]. This underscores the intertwined relationship between hypoxia and the Wnt signaling pathway. In addition, it renders these pathways, the key nodes in the networks and their interactions an attractive potential therapeutic target for OA.

Acknowledgments

We are grateful to L. Storms for her technical support of this study and for, together with A. Hens, taking care of the animal facility management. We thank I. Jonkers and J. Peeters for making the hypoxia incubator available. We are indebted to the UZ Leuven nursing staff for their efforts to provide cartilage samples for *ex vivo* and *in vitro* work.

Author contributions

J.Q, A.D.R, R.J.L. and S.M. planned the study and designed all the *in vitro*, *ex vivo*, and *in vivo* experiments. F.M.F.C. performed the animal experiments. J.Q, A.D.R. and A.E.N. performed the *in vitro* experiments. J.Q., S.P. and R.J.L. are responsible for all the statistical analyses. A.S provided essential materials. J.Q., S.M. and R.J.L. wrote the manuscript.

Role of the funding source

This work was supported by grants from the Flanders Research Foundation (FWO-Vlaanderen) (11A7320N), a KU Leuven Starting Grant (D7014), and Excellence of Science (G0F8218N, Joint-against-OA) programs. J.Q. is recipient of a fundamental research PhD fellowship from FWO-Vlaanderen.

Competing interest statement

Leuven Research and Development, the technology transfer office of KU Leuven, has received consultancy and speaker fees and research grants on behalf of R.J.L. from Abbvie, Boehringer-

Ingelheim, Amgen (Celgene), Eli-Lilly, Galapagos, Janssen, MSD, Novartis, Pfizer, Biosplice Therapeutics (formerly Samumed), and UCB. The other authors declare that they have no competing financial interests.

References

1. Cornelis FMF, Monteagudo S, Guns LKA, den Hollander W, Nelissen R, Storms L, et al. ANP32A regulates ATM expression and prevents oxidative stress in cartilage, brain, and bone. Sci Transl Med 2018; 10.
2. Reilly PT, Yu Y, Hamiche A, Wang L. Cracking the ANP32 whips: important functions, unequal requirement, and hints at disease implications. Bioessays 2014; 36: 1062-1071.
3. Monteagudo S, Cornelis FMF, Wang X, de Roover A, Peeters T, Quintiens J, et al. ANP32A represses Wnt signaling across tissues thereby protecting against osteoarthritis and heart disease. Osteoarthritis Cartilage 2022; 30: 724-734.
4. Valdes AM, Loughlin J, Timms KM, van Meurs JJ, Southam L, Wilson SG, et al. Genome-wide association scan identifies a prostaglandin-endoperoxide synthase 2 variant involved in risk of knee osteoarthritis. Am J Hum Genet 2008; 82: 1231-1240.
5. Valdes AM, Lories RJ, van Meurs JB, Kerkhof H, Doherty S, Hofman A, et al. Variation at the ANP32A gene is associated with risk of hip osteoarthritis in women. Arthritis Rheum 2009; 60: 2046-2054.
6. Lories RJ, Corr M, Lane NE. To Wnt or not to Wnt: the bone and joint health dilemma. Nat Rev Rheumatol 2013; 9: 328-339.
7. Zhu M, Tang D, Wu Q, Hao S, Chen M, Xie C, et al. Activation of beta-catenin signaling in articular chondrocytes leads to osteoarthritis-like phenotype in adult beta-catenin conditional activation mice. J Bone Miner Res 2009; 24: 12-21.
8. De Roover A, Núñez AE, Cornelis FM, Cherifi C, Casas-Fraile L, Sermon A, et al. Hypoxia induces DOT1L in articular cartilage to protect against osteoarthritis. JCI Insight 2021; 6.

9. Sandelin A, Wasserman WW, Lenhard B. ConSite: web-based prediction of regulatory elements using cross-species comparison. Nucleic Acids Res 2004; 32: W249-252.
10. Ghosh D. Object-oriented transcription factors database (ooTFD). Nucleic Acids Res 2000; 28: 308-310.
11. Livyatan I, Aaronson Y, Gokhman D, Ashkenazi R, Meshorer E. BindDB: An Integrated Database and Webtool Platform for "Reverse-ChIP" Epigenomic Analysis. Cell Stem Cell 2015; 17: 647-648.
12. Messeguer X, Escudero R, Farré D, Núñez O, Martínez J, Albà MM. PROMO: detection of known transcription regulatory elements using species-tailored searches. Bioinformatics 2002; 18: 333-334.
13. Dreos R, Ambrosini G, Périer RC, Bucher P. The Eukaryotic Promoter Database: expansion of EPDnew and new promoter analysis tools. Nucleic Acids Res 2015; 43: D92-96.
14. Oshchepkov DY, Levitsky VG. In Silico Prediction of Transcriptional Factor-Binding Sites. In: In Silico Tools for Gene Discovery, Yu B, Hinchcliffe M Eds.: Humana Press 2011.
15. Jayaram N, Usvyat D, AC RM. Evaluating tools for transcription factor binding site prediction. BMC Bioinformatics 2016; 17: 547.
16. Szklarczyk D, Gable AL, Lyon D, Junge A, Wyder S, Huerta-Cepas J, et al. STRING v11: protein-protein association networks with increased coverage, supporting functional discovery in genome-wide experimental datasets. Nucleic Acids Res 2019; 47: D607-d613.
17. Greene CS, Krishnan A, Wong AK, Ricciotti E, Zelaya RA, Himmelstein DS, et al. Understanding multicellular function and disease with human tissue-specific networks. Nat Genet 2015; 47: 569-576.

517 18. Krämer A, Green J, Pollard J, Jr., Tugendreich S. Causal analysis approaches in
518 Ingenuity Pathway Analysis. Bioinformatics 2014; 30: 523-530.
519 19. Goldring MB, Birkhead JR, Suen LF, Yamin R, Mizuno S, Glowacki J, et al.
520 Interleukin-1 beta-modulated gene expression in immortalized human chondrocytes. J
521 Clin Invest 1994; 94: 2307-2316.
522 20. Monteagudo S, Cornelis FMF, Aznar-Lopez C, Yibmantasiri P, Guns LA, Carmeliet
523 P, et al. DOT1L safeguards cartilage homeostasis and protects against osteoarthritis.
524 Nat Commun 2017; 8: 15889.
525 21. Glasson SS, Blanchet TJ, Morris EA. The surgical destabilization of the medial
526 meniscus (DMM) model of osteoarthritis in the 129/SvEv mouse. Osteoarthritis
527 Cartilage 2007; 15: 1061-1069.
528 22. Lories RJ, Peeters J, Bakker A, Tylzanowski P, Derese I, Schrooten J, et al. Articular
529 cartilage and biomechanical properties of the long bones in Frzb-knockout mice.
530 Arthritis Rheum 2007; 56: 4095-4103.
531 23. Jensen EC. Quantitative Analysis of Histological Staining and Fluorescence Using
532 ImageJ. The Anatomical Record 2013; 296: 378-381.
533 24. Schneider CA, Rasband WS, Eliceiri KW. NIH Image to ImageJ: 25 years of image
534 analysis. Nature Methods 2012; 9: 671-675.
535 25. Thoms BL, Dudek KA, Lafont JE, Murphy CL. Hypoxia promotes the production and
536 inhibits the destruction of human articular cartilage. Arthritis Rheum 2013; 65: 1302-
537 1312.
538 26. Okada K, Mori D, Makii Y, Nakamoto H, Murahashi Y, Yano F, et al. Hypoxia-
539 inducible factor-1 alpha maintains mouse articular cartilage through suppression of
540 NF-κB signaling. Sci Rep 2020; 10: 5425.

27. Choudhry H, Harris AL. Advances in Hypoxia-Inducible Factor Biology. Cell Metab 2018; 27: 281-298.
28. Kaelin WG, Jr., Ratcliffe PJ. Oxygen sensing by metazoans: the central role of the HIF hydroxylase pathway. Mol Cell 2008; 30: 393-402.
29. Castro-Mondragon JA, Riudavets-Puig R, Rauluseviciute I, Berhanu Lemma R, Turchi L, Blanc-Mathieu R, et al. JASPAR 2022: the 9th release of the open-access database of transcription factor binding profiles. Nucleic Acids Res 2022; 50: D165-d173.
30. Lories RJ, Monteagudo S. Review Article: Is Wnt Signaling an Attractive Target for the Treatment of Osteoarthritis? Rheumatol Ther 2020; 7: 259-270.
31. Monteagudo S, Lories RJ. Cushioning the cartilage: a canonical Wnt restricting matter. Nat Rev Rheumatol 2017; 13: 670-681.
32. Lories RJ, Peeters J, Szlufcik K, Hespel P, Luyten FP. Deletion of frizzled-related protein reduces voluntary running exercise performance in mice. Osteoarthritis Cartilage 2009; 17: 390-396.
33. Cadigan KM, Waterman ML. TCF/LEFs and Wnt signaling in the nucleus. Cold Spring Harb Perspect Biol 2012; 4.
34. Chowdhury R, Candela-Lena JI, Chan MC, Greenald DJ, Yeoh KK, Tian YM, et al. Selective small molecule probes for the hypoxia inducible factor (HIF) prolyl hydroxylases. ACS Chem Biol 2013; 8: 1488-1496.
35. Zhang FJ, Luo W, Lei GH. Role of HIF-1α and HIF-2α in osteoarthritis. Joint Bone Spine 2015; 82: 144-147.
36. Bouaziz W, Sigaux J, Modrowski D, Devignes CS, Funck-Brentano T, Richette P, et al. Interaction of HIF1alpha and beta-catenin inhibits matrix metalloproteinase 13

565 expression and prevents cartilage damage in mice. Proc Natl Acad Sci U S A 2016;
566 113: 5453-5458.
567 37. Markway BD, Cho H, Zilberman-Rudenko J, Holden P, McAlinden A, Johnstone B.
568 Hypoxia-inducible factor 3-alpha expression is associated with the stable chondrocyte
569 phenotype. J Orthop Res 2015; 33: 1561-1570.
570 38. Li VS, Ng SS, Boersema PJ, Low TY, Karthaus WR, Gerlach JP, et al. Wnt signaling
571 through inhibition of β-catenin degradation in an intact Axin1 complex. Cell 2012;
572 149: 1245-1256.
573 39. Huang SM, Mishina YM, Liu S, Cheung A, Stegmeier F, Michaud GA, et al.
574 Tankyrase inhibition stabilizes axin and antagonizes Wnt signalling. Nature 2009;
575 461: 614-620.
576 40. Guleria A, Chandna S. ATM kinase: Much more than a DNA damage responsive
577 protein. DNA Repair (Amst) 2016; 39: 1-20.
578 41. Jeon OH, Kim C, Laberge RM, Demaria M, Rathod S, Vasserot AP, et al. Local
579 clearance of senescent cells attenuates the development of post-traumatic osteoarthritis
580 and creates a pro-regenerative environment. Nat Med 2017; 23: 775-781.
581 42. Liu Y, Molchanov V, Yang T. Enzymatic Machinery of Ubiquitin and Ubiquitin-Like
582 Modification Systems in Chondrocyte Homeostasis and Osteoarthritis. Curr
583 Rheumatol Rep 2021; 23: 62.
584 43. Schipani E, Ryan HE, Didrickson S, Kobayashi T, Knight M, Johnson RS. Hypoxia in
585 cartilage: HIF-1alpha is essential for chondrocyte growth arrest and survival. Genes
586 Dev 2001; 15: 2865-2876.
587 44. Hu S, Zhang C, Ni L, Huang C, Chen D, Shi K, et al. Stabilization of HIF-1α
588 alleviates osteoarthritis via enhancing mitophagy. Cell Death Dis 2020; 11: 481.

45. Yazici Y, McAlindon TE, Gibofsky A, Lane NE, Clauw D, Jones M, et al. Lorecivivint, a Novel Intraarticular CDC-like Kinase 2 and Dual-Specificity Tyrosine Phosphorylation-Regulated Kinase 1A Inhibitor and Wnt Pathway Modulator for the Treatment of Knee Osteoarthritis: A Phase II Randomized Trial. Arthritis Rheumatol 2020; 72: 1694-1706.

FIGURE LEGENDS

Figure 1. Identification of transcription factors regulating the ANP32A gene using bioinformatics. (**A**) Schematic overview of the bioinformatic analysis pipeline applied to the human *ANP32A* proximal promoter. The upper part of figure A shows the *ANP32A* gene promoter region that was used for the analysis; -1000 basepairs (bp) to +100 bp relative to the transcription start site (TSS). The lower part displays the 4 different bioinformatics web-based tools that were interrogated and the selection process for the transcription factors (TFs). (**B**) Venn diagram representing 49 TFs predicted by at least 2 different tools. (**C**) Overview of the 16 remaining TFs after specificity analysis. Two different approaches were applied to determine which TFs were more specific for the *ANP32A* promoter as compared to the aggrecan (*ACAN*), collagen 2a1 (*COL2A1*), and actin (*ACTB*) promoters. The diagram in C shows the 16 remaining TFs that were predicted to be more specific for *ANP32A* by the two approaches and their overlap.

Figure 2. Bioinformatics analysis of the ANP32A promoter suggests that the Wnt signaling and the hypoxia pathway regulate ANP32A expression. (A) Cartilage-specific gene network obtained with the HumanBase network analysis using the 49 transcription factors (TFs). Module 4 (M4) represents the hypoxia pathway. **(B)** STRING database analysis of the 49 TFs showing the Wnt signaling pathway as one of the enriched pathways. TFs in red are related to the Wnt signaling pathway. **(C)** Ingenuity pathway analysis (IPA) of the 49 TFs. **(D)** The presence of a hypoxia response element (HRE) with consensus sequence 5'-(A/G)CGTG-3' in the promoter of *ANP32A*. Since the *ANP32A* gene is oriented on the reverse strand of the DNA (Ensembl release 105), this HRE is found in the reverse complement 5'-CACG(C/T)-3'. The position is indicated by the basepairs (bp) relative to the transcription start site (TSS). (**E**)

The presence of two Wnt response elements (WRE) in the promoter of *ANP32A* (one in the reverse complement). The position is indicated by the bp relative to the TSS.

Figure 3. Hypoxia increases ANP32A expression in chondrocytes and in an OA mouse model. (**A**) Real-time PCR for *ANP32A* and *VEGF* in C28/I2 cells treated with hypoxia mimetic IOX2 or vehicle (V) for 72 hours (n = 4 independent experiments with three technical replicates, mean ± SD, p=0.18 and p=0.21 with 20µM and 50 µM IOX2 respectively for *ANP32A* and p<0.0001 with 20 µM and 50 µM IOX2 for *VEGF* Dunnett-corrected for two tests in one-way ANOVA). (**B**) Real-time PCR for *ANP32A* and *VEGF* in C28/I2 cells in normoxic (21% O2) or hypoxic (1% O2) conditions for 6 hours (n = 3 independent experiments with three technical replicates, mean ± SD, p=0.01 by unpaired t-test for *ANP32A* and p=0.0003 for *VEGF*). (**C**) Western blot analysis of ANP32A, HIF1A and actin in C28/I2 cells treated with hypoxia mimetic IOX2 for 72 hours. Images are representative of 2 independent experiments. (**D**) Western blot analysis of ANP32A, HIF1A and actin in C28/I2 cells in normoxic (21% O2) or hypoxic (1% O2) conditions for 6 hours and 24 hours respectively. Images are representative of 2 independent experiments. (**E**) Real-time PCR for *ANP32A* and *VEGF* in primary human articular chondrocytes treated with hypoxia mimetic IOX2 (20 µM) or vehicle (V) for 72 hours (n = 5 independent experiments with three technical replicates, mean ± SD, p=0.01 for *ANP32A* and p=0.0004 for *VEGF* by paired t-test). The dosage of 50 µM was omitted since it showed toxicity in the primary human articular chondrocytes in a previous study. (**F**) Real-time PCR for *ANP32A* and *VEGF* in primary human articular chondrocytes in normoxic (21% O2) or hypoxic (1% O2) conditions for 14 days (n = 5 independent experiments with three technical replicates, mean ± SD, p=0.0009 for *ANP32A* and p=0.002 for *VEGF* by paired t-test). (**G**) Immunohistochemical staining for ANP32A protein in the articular cartilage of wild-type mice after intra-articular injection with IOX2 (0.5 mg/kg) or vehicle (V) after destabilization of the

medial meniscus surgery (DMM) or sham surgery (SHAM). Scale bar: 50 µm. A quantification is shown in the right part of the panel (n = 5 mice per group, mean ± SD, p=0.0002 for comparison between the DMM + IOX2 group and the DMM + vehicle group and p<0.0001 for the comparison between the DMM + vehicle group and the sham + vehicle group Dunnett-corrected for 3 tests in one-way ANOVA). (**H**) Chromatin immunoprecipitation quantitative PCR (ChIP-qPCR) for HIF1A and HIF2A binding to *ANP32A* and *VEGF* promoters in C28/I2 cells treated with IOX2 (20 µM) for 72 hours (n = 3 independent experiments with three technical replicates, mean ± SD, p=0.02 and p=0.04 respectively for HIF1A in the *ANP32A* and *VEGF* assay and p=0.22 and p=0.26 respectively for HIF2A in the *ANP32A* and *VEGF* assay by one sample t-test).

Figure 4. Hyper-activation of Wnt signaling decreases ANP32A expression in articular cartilage. (**A**) Real-time PCR for *ANP32A* and Wnt target gene *TCF1* in primary human articular chondrocytes treated with Wnt activator CHIR99021 (CHIR, 3 µM) or vehicle (DMSO) for 24 hours (n = 5 independent experiments with three technical replicates, mean ± SD, p=0.04 for *ANP32A* and p<0.0001 for *VEGF* by paired t-test). (**B**) Immunohistochemical staining for ANP32A protein in the articular cartilage of wild-type mice treated with CHIR99021 (1 mg/kg) or vehicle. Scale bar: 50 µm. A quantification is shown in the right part of the panel (n = 3 mice per group, mean ± SD, p=0.0037 by unpaired t-test). (**C**) Immunohistochemical staining for ANP32A protein in the articular cartilage of wild-type littermates (WT) and *Frzb*-knockout mice. Scale bar: 50 µm. A quantification is shown in the right part of the panel (n = 5 mice per group, mean ± SD, p=0.05 by unpaired t-test). (**D**) Immunohistochemical staining for ANP32A protein in the articular cartilage of wild-type mice treated with XAV939 or vehicle. Scale bar: 50 µm. A quantification is shown in the right part of the panel (n = 3 mice per group, mean ± SD, p<0.0001 by unpaired t-test).

Figure 5: Modulation of hypoxia and Wnt signaling lead to ANP32A downstream changes in the articular chondrocyte. (**A**) Real-time PCR for *ATM*, directly regulated by ANP32A, in primary human articular chondrocytes treated with hypoxia mimetic IOX2 (20 μM) or vehicle (DMSO) for 72 hours (n = 5 independent experiments with three technical replicates, mean ± SD, p=0.02). (**B**) Real-time PCR for *ATM* in primary human articular chondrocytes in normoxic (21% O2) or hypoxic (1% O2) conditions for 7 to 14 days (n = 5 independent experiments with three technical replicates, mean ± SD, p=0.01). (**C**) Real-time PCR for *ATM*, directly regulated by ANP32A, in primary human articular chondrocytes treated with Wnt activator CHIR99021 (CHIR, 3 μM) or vehicle (DMSO) for 24 hours (n = 5 independent experiments with three technical replicates, mean ± SD, p=0.04 for ANP32A by paired t-test). (**D**) Scheme summarizing the effect of hypoxia and Wnt signaling on *ANP32A* expression, *ATM* expression and cartilage health.

Figure 1

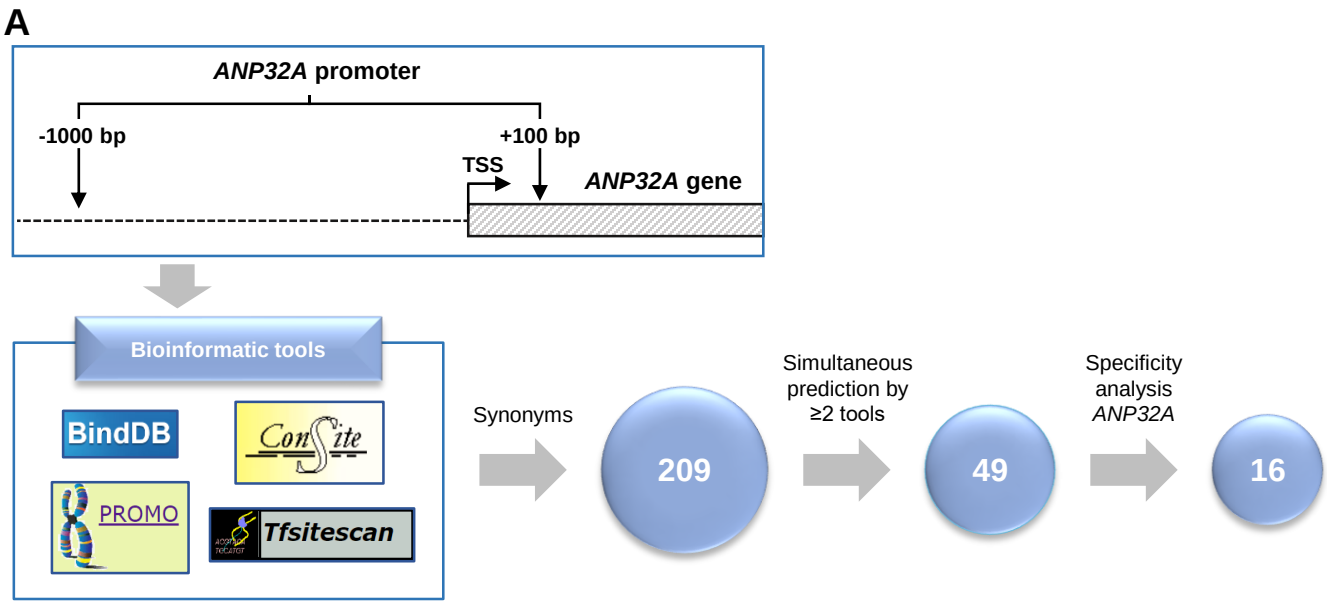
A
ANP32A promoter
-1000 bp
+100 bp
TSS
ANP32A gene
Bioinformatic tools
BindDB
Consite
PROMO
Tfsitescan
Synonyms
209
Simultaneous prediction by ≥2 tools
49
Specificity analysis ANP32A
16

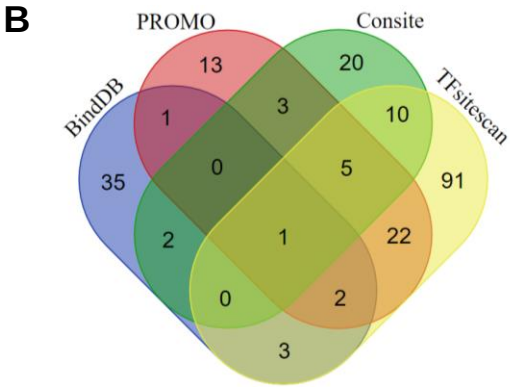
B
PROMO
Consite
BindDB
TFsitescan
13
20
1
3
10
35
0
5
91
2
1
22
0
2
3

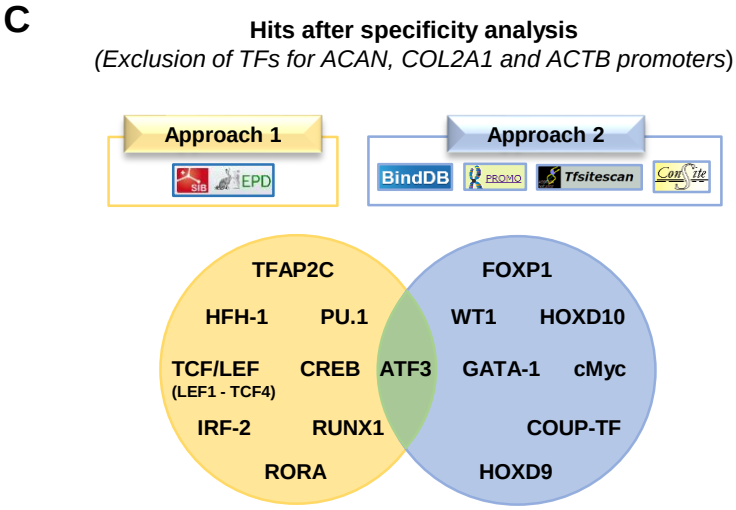
C
Hits after specificity analysis
(Exclusion of TFs for ACAN, COL2A1 and ACTB promoters)
Approach 1
EPD
Approach 2
BindDB
PROMO
Tfsitescan
Consite
TFAP2C
HFH-1
PU.1
TCF/LEF
(LEF1 - TCF4)
CREB
IRF-2
RUNX1
RORA
ATF3
FOXP1
WT1
HOXD10
GATA-1
cMyc
COUP-TF
HOXD9

Figure 2

A

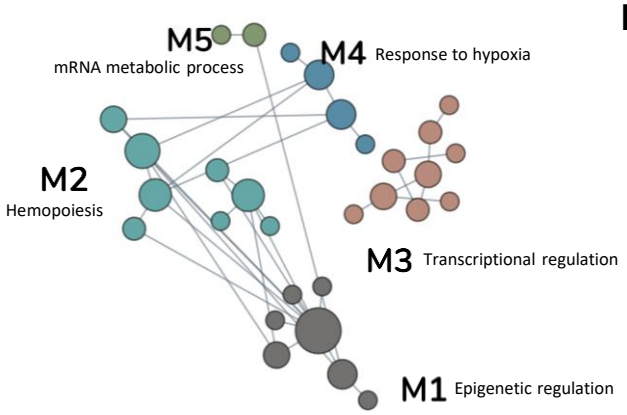

B

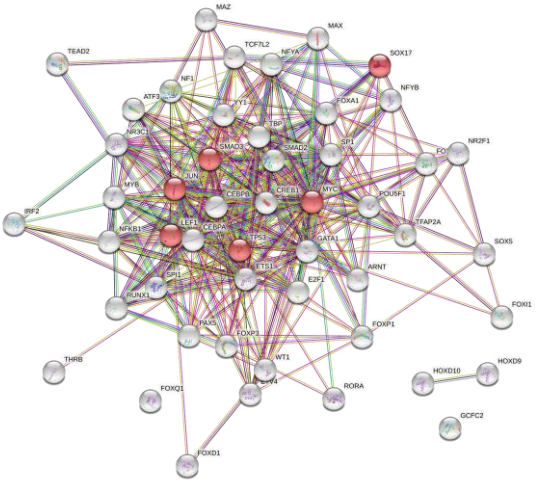

C

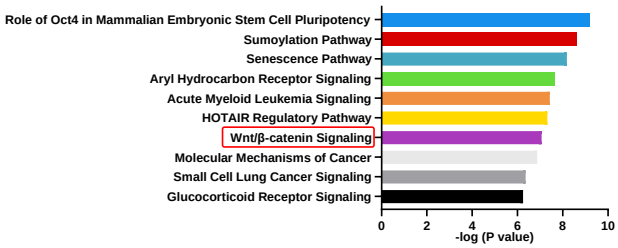

D

HRE in ANP32A promoter

5’- AGC**CACGC**TCC - 3’

-601 -591 bp relative to TSS

E

WRE in ANP32A promoter

5’- AGC**CTTCAAAG**TCC - 3’

49 62 bp relative to TSS

5’- AGG**CCTTTCATC**TGC - 3’

-517 -503 bp relative to TSS

Figure 3

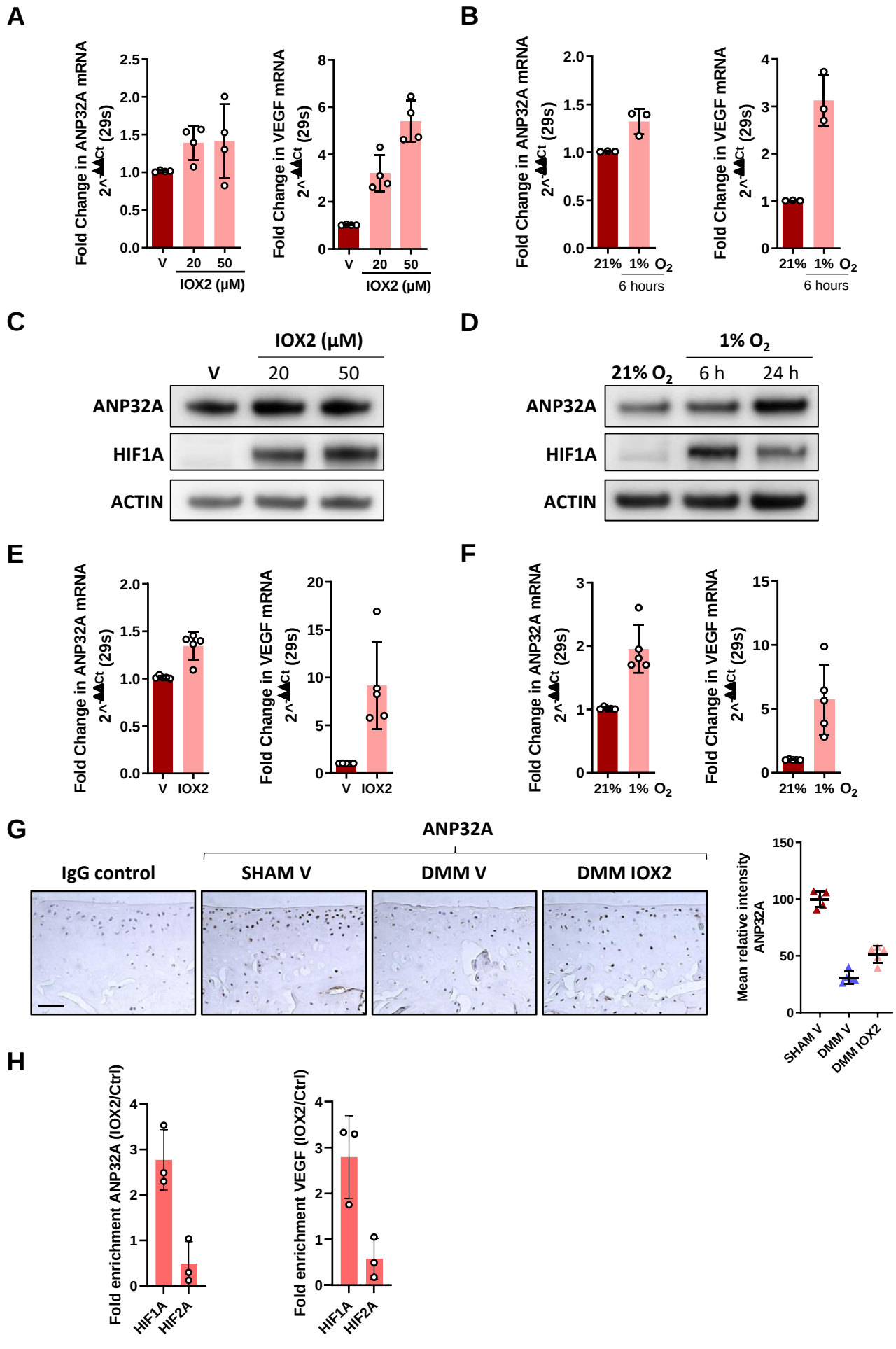
A
Fold Change in ANP32A mRNA 2^-ΔΔCt (29s)
V
20
50
IOX2 (μM)
Fold Change in VEGF mRNA 2^-ΔΔCt (29s)
B
21%
1% O2
6 hours
C
IOX2 (μM)
ANP32A
HIF1A
ACTIN
D
1% O2
21% O2
6 h
24 h
E
IOX2
F
G
ANP32A
IgG control
SHAM V
DMM V
DMM IOX2
Mean relative intensity ANP32A
H
Fold enrichment ANP32A (IOX2/Ctrl)
Fold enrichment VEGF (IOX2/Ctrl)
HIF1A
HIF2A

Figure 4

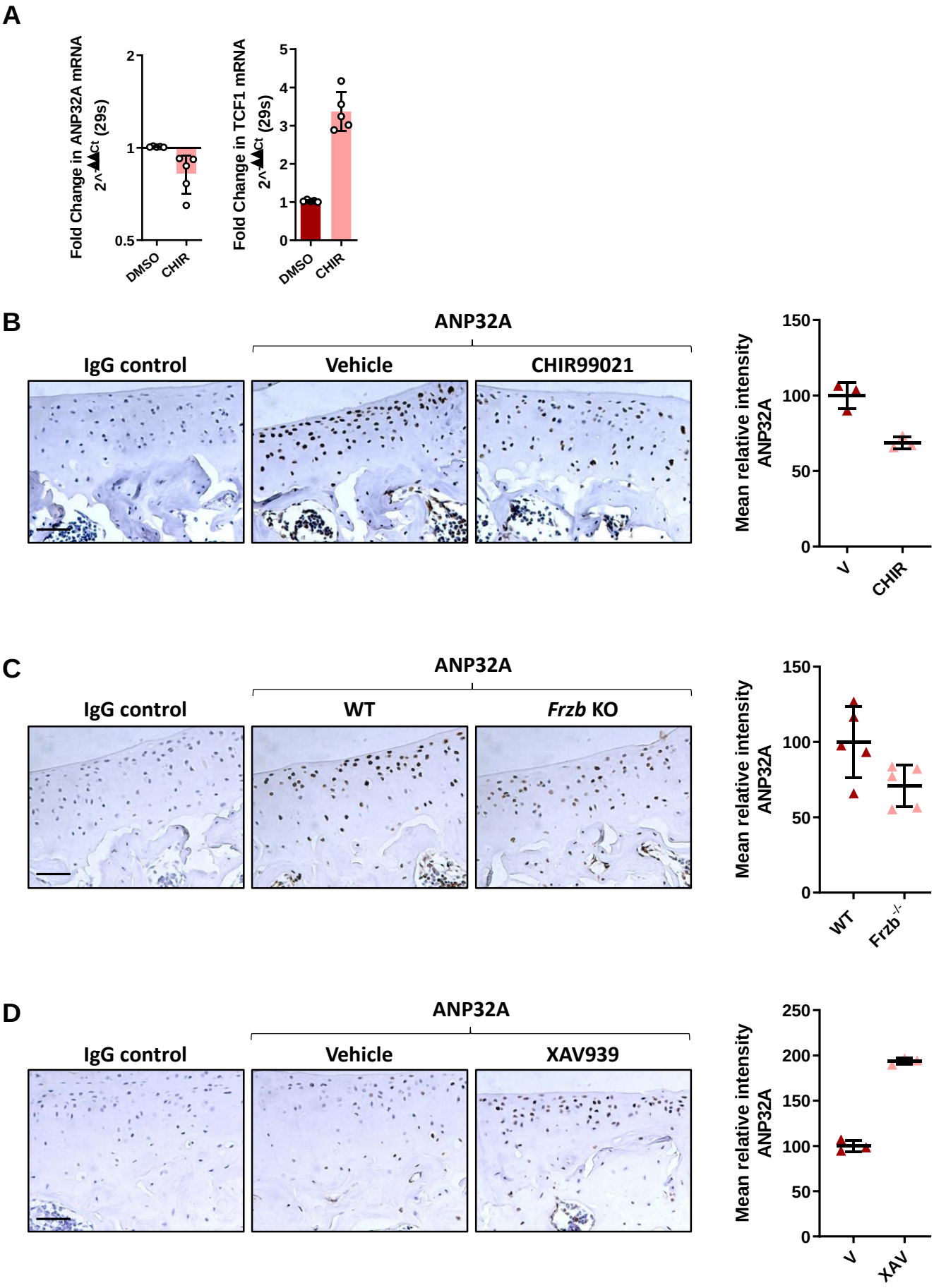
A
Fold Change in ANP32A mRNA
2^-ΔΔCt (29s)
2
1
0.5
DMSO
CHIR
Fold Change in TCF1 mRNA
2^-ΔΔCt (29s)
5
4
3
2
1
0
DMSO
CHIR
B
ANP32A
IgG control
Vehicle
CHIR99021
Mean relative intensity
ANP32A
150
100
50
0
V
CHIR
C
ANP32A
IgG control
WT
Frzb KO
Mean relative intensity
ANP32A
150
100
50
0
WT
Frzb -/-
D
ANP32A
IgG control
Vehicle
XAV939
Mean relative intensity
ANP32A
250
200
150
100
50
0
V
XAV

Figure 5

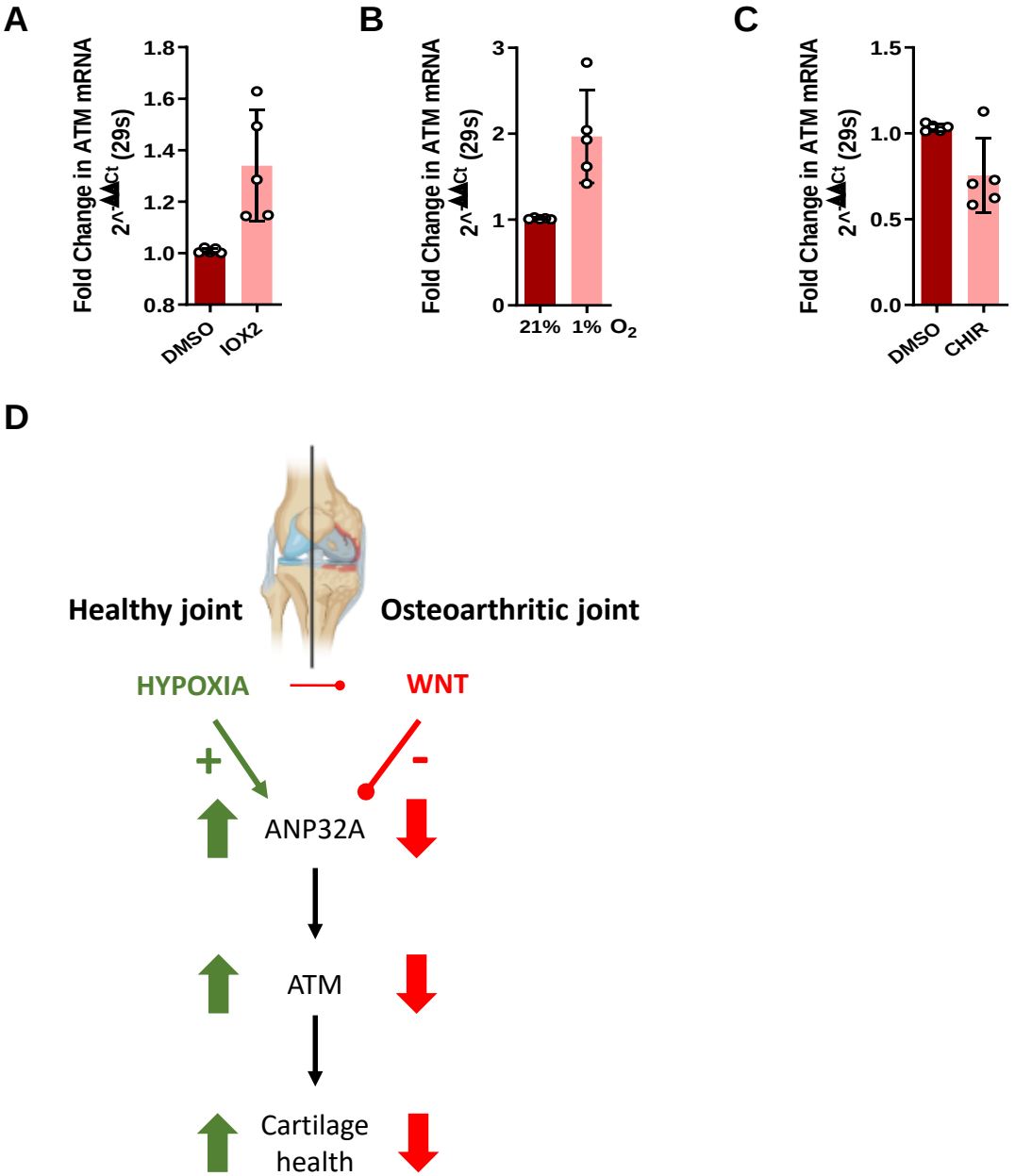
A
Fold Change in ATM mRNA
2^-ΔΔCt (29s)
1.8
1.6
1.4
1.2
1.0
0.8
DMSO
IOX2
B
Fold Change in ATM mRNA
2^-ΔΔCt (29s)
3
2
1
0
21%
1% O2
C
Fold Change in ATM mRNA
2^-ΔΔCt (29s)
1.5
1.0
0.5
0.0
DMSO
CHIR
D
Healthy joint
Osteoarthritic joint
HYPOXIA
WNT
+
-
ANP32A
ATM
Cartilage health

SUPPLEMENTARY FIGURE LEGENDS

Figure S1: Treatment with IOX2 in vivo increases HIF1A. Immunohistochemical staining for HIF1A protein in the articular cartilage of wild-type mice treated with IOX2 (0.5 mg/kg) or vehicle (V) after destabilization of the medial meniscus surgery (DMM) or sham surgery (SHAM). Scale bar: 50 µm.

Figure S2: Wnt overexpression and Wnt inhibition in in vivo models. (**A**) Immunohistochemical staining for TCF1 protein, a direct Wnt target gene, in the articular cartilage of wild-type mice treated with CHIR99021 (1 mg/kg) or vehicle (V). Scale bar: 50 µm. A quantification is shown in the right part of the panel (n = 3 mice per group, mean ± SD, p=0.0006 by unpaired t-test). (**B**) Immunohistochemical staining for TCF1 protein, a direct Wnt target gene, in the articular cartilage of wild-type littermates (WT) and *Frzb*-knockout mice (KO). Scale bar: 50 µm. A quantification is shown in the right part of the panel (n = 3 mice per group, mean ± SD, p=0.0006 by unpaired t-test). (**C**) Immunohistochemical staining for TCF1 protein, a direct Wnt target gene, in the articular cartilage of wild-type mice treated with XAV939 or vehicle. Scale bar: 50 µm. A quantification is shown in the right part of the panel (n = 3 mice per group, mean ± SD, p=0.001 by unpaired t-test).

SUPPLEMENTARY TABLE LEGENDS

Supplementary Table 1: Patient characteristics. (**A**) Primary human articular chondrocytes used for the experiments with IOX2 (Figure 3E and Figure 5A). (**B**) Primary human articular chondrocytes used for the experiments in the hypoxia incubator (Figure 3F and Figure 5B). (**C**) Primary human articular chondrocytes used for the treatment with CHIR99021 (Figure 4A and Figure 5C).

Supplementary Table 2: Bioinformatic analysis pipeline results. (**A**) ANP32A proximal promoter sequence (1000 basepairs (bp) upstream and 100 basepairs downstream relative to the transcription start site (TSS). (**B**) Table with the 49 final transcription factors that were simultaneously predicted by at least two databases. (**C**) Table with the 16 final hits after specificity analysis, obtained with approach A, approach B and the hit that was presented with both approaches (A+B). (**D**) The 5 modules as predicted by the network analysis performed with the HumanBase tool.

Supplementary Table 3: Human primers used in qPCR analysis.

Supplementary Table 4: Animal experiments: Overview, setup and analysis details. Abbreviations: CHIR99021 (CHIR), destabilization of the medial meniscus (DMM), immunohistochemistry (IHC), intra-articular (i.a.), knockout (KO), osteoarthritis (OA), wild-type (WT), XAV939 (XAV).

Figure S1

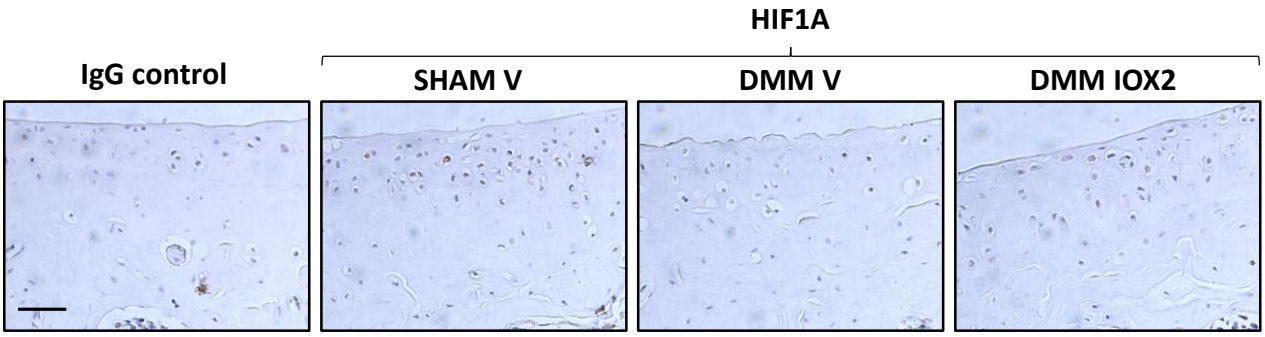

Figure S2

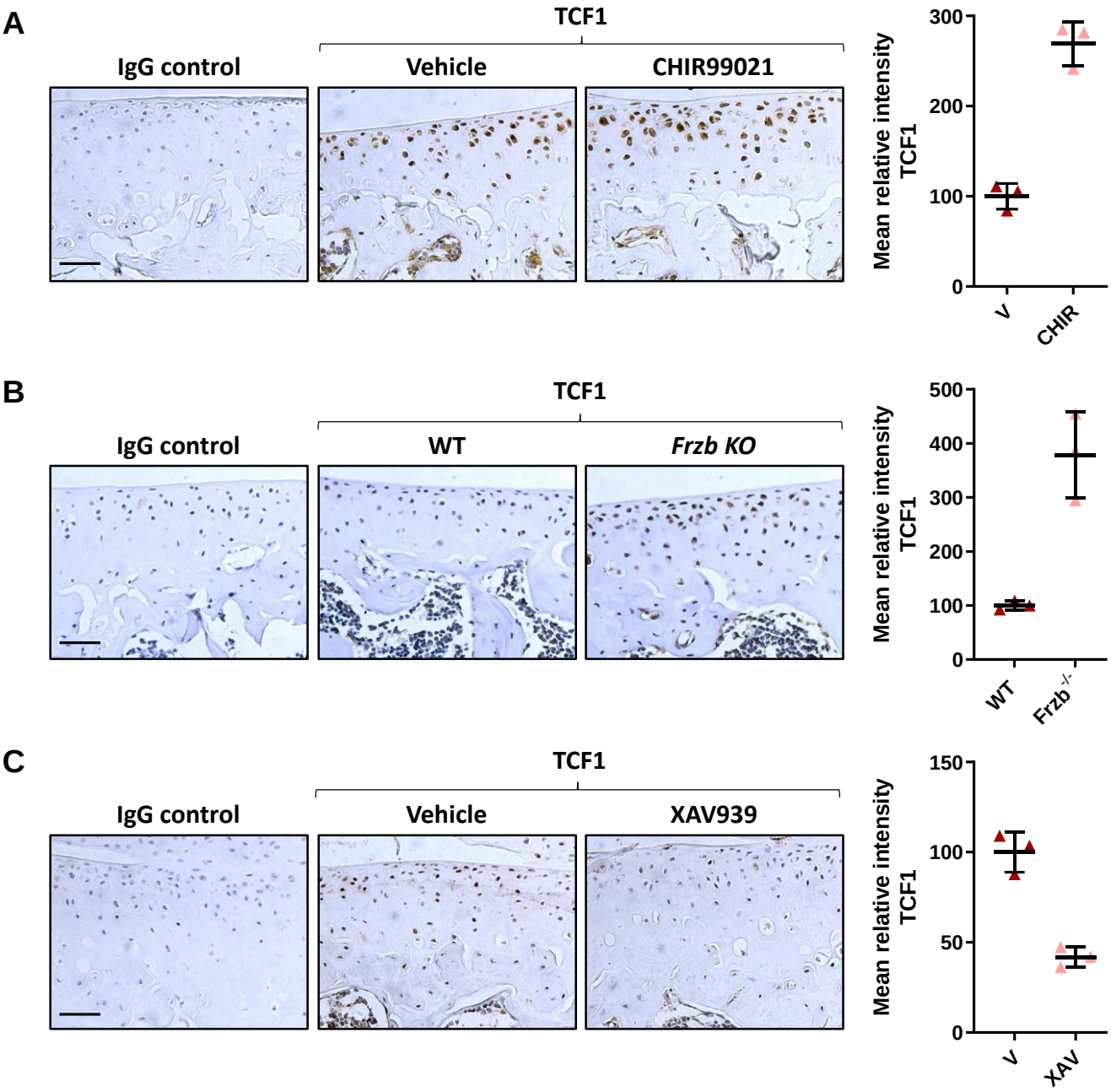
A
TCF1
IgG control
Vehicle
CHIR99021
Mean relative intensity TCF1
300
200
100
0
V
CHIR
B
TCF1
IgG control
WT
Frzb KO
Mean relative intensity TCF1
500
400
300
200
100
0
WT
Frzb -/-
C
TCF1
IgG control
Vehicle
XAV939
Mean relative intensity TCF1
150
100
50
0
V
XAV

Supplementary Table 1

A

Patient number	Age (years)	Gender
P146	69	Male
P161	89	Female
P194	91	Female
P320	90	Male
P324	94	Female

B

Patient number	Age (years)	Gender
P183	94	Female
P185	92	Female
P194	91	Female
P320	90	Male
P324	94	Female

C

Patient number	Age (years)	Gender
P127	93	Female
P140	91	Female
P221	89	Female
P291	68	Male
P298	70	Female

Supplementary Table 2

A

AACCGTGCGCCGTTCTCTTTCACTAGGTCTATAAAGCCCAGAAATTATGTTTGGTCCAGAAAACCAGGAGTTATGA
GCACCTTCCTTTTCCACCTTTTAATATTCTACATATCTAGCAACGGTTCTTAATCCATGGTCTTCATTCATTTATTGCC
TAAACAAGATCTTGGGTGTCTCTTGGTGATCACTTCTTCCAAGCTGACCTAATATGACAGCAAAGTGAAAAGCCTC
TTCGTGGGAAGGGTCGCGACCGCGCGGTAAGTCATCCAAAAGTGGAAGCATCTTGCTTTTACTGACTTATGTATA
CGAGGGTGGCGATGGTGGCGGCCTGACAGGGACGAGGCCGGAGGGGAAGGGGCGCGCGGGCTGCTGGGCAG
CCGCGGTGGGGGTGACGGGGGCAGCCACGCTCCCCAGCGCGAGCCGCCGGACCCGGGACCCGACGAGCCCCTC
CCGGCATTGCACCCTGACCCCTCTCCTCCTTCCAGGCCTTTCATCTGCCCTCCCGCTGGGCAGCCCGCGGTCCCCGG
ACCTCAAGCCGCCCGCCTCCTTCCGCAACCCCGTCGCGCCGCCCCGCGAAGCCCTCGGCCGGGCGGGGACCCCGA
CCCGACCCCTCCGGCCGCGCCCCTCCCCCTCGCAGAACGCACCTGCGGCCCCGCCCCCGGCCGAACGCTGAGGCG
GCGGCTGGCTGGCAAGGCCGGGCGGCTCGGCCCTCGAGGCACAGTCACCTTCCCTTCCCCCGCCATTCCGCCCAC
CCCCCTCACTCAGCCACAGAGCAGCCGCCGCGCTCCTCAGCCGCCCCGAAATCTAAAGGGGTCCGTCTCCGGCAC
CACTACCAAATGGCCGAGCCTCCCTGGCCGGCTGCGCAGCCCGCCCATTGGTCCCTTCCCCCCCCCGCCGCCACTG
CCATTGGCTGTTGCCCGGAGACCCTCGGCGGCGATTGGCTCGGGCCGCTGCCGCTCGTCCATGGGGCCGCAGAT
CCCGCCTCCACGGCGATCAGGTTAGTGTGCGCCGCGGGTGCTGGGGGCTCGAGAACCGAGCGGAGCTGGTTGA
GCCTTCAAAGTCCTAAAACGCGCGGCCGTGGGTTCGGGGTTTATTGATTGA

B

49 hits	
cMyc	PEA3
E2f	AP-2
Max	MAZ
CREB	ETF
Oct 3/4	Sp1
FOXP1	NF-kappaB1
P53	WT1
TBP	T3R-beta1
Pax-5	NF-Y
C/EBPbeta	HNF3A
NF-1	TCF/LEF
FOXP3	COUP-TF
GATA-1	c-Ets
YY1	c-Myb
C/EBPalpha	RORA
PU.1	HFH-2
ATF3	HFH-3
HOXD9	SOX17
HOXD10	HFH-1
SRY	FREAC-4
GR	Sox-5
IRF-2	SRF
GCF	RUNX1
AP-1	ARNT
SMAD 2/3	

C

16 final hits		
Approach A	**Approach A+B**	**Approach B**
TFAP2C	ATF3	cMyc
CREB		COUP-TF
HFH-1		GATA-1
IRF-2		HOXD10
PU.1		HOXD9
RORA		WT1
RUNX1		FOXP1
TCF/LEF (LEF1, TCF4)		

D

Module	Top Terms	Q val	Genes
M1	pri-miRNA transcription by RNA polymerase II	0.00001970	7
	positive regulation of pri-miRNA transcription by RNA polymerase II	0.00061249	
	regulation of pri-miRNA transcription by RNA polymerase II	0.00062525	
	regulation of histone modification	0.00179384	
	modification of morphology or physiology of other organism involved in symbiotic interaction	0.00189795	
	transforming growth factor beta receptor signaling pathway	0.00221093	
	regulation of chromatin organization	0.00221093	
	cellular response to transforming growth factor beta stimulus	0.00309352	
	modification of morphology or physiology of other organism	0.00309352	
	response to transforming growth factor beta	0.00319392	
M2	positive regulation of transcription from RNA polymerase II promoter in response to endoplasmic reticulum stress	0.00025507	8
	positive regulation of transcription from RNA polymerase II promoter in response to stress	0.00062017	
	regulation of transcription from RNA polymerase II promoter in response to stress	0.00108945	
	regulation of DNA-templated transcription in response to stress	0.00108945	
	positive regulation of myeloid cell differentiation	0.00168345	
	positive regulation of hemopoiesis	0.00215740	
	regulation of myeloid cell differentiation	0.00238363	
	regulation of hemopoiesis	0.00420518	
	myeloid cell differentiation	0.00471543	
	response to endoplasmic reticulum stress	0.00479646	
M3	regulation of transcription by RNA polymerase III	0.00061249	9
	transcription by RNA polymerase III	0.00076729	
	cell fate commitment	0.00108945	
	transcription initiation from RNA polymerase II promoter	0.00108945	
	DNA-templated transcription, initiation	0.00179384	
	response to wounding	0.00543480	
	cellular response to hormone stimulus	0.00927450	
	response to hormone	0.01090200	
M4	response to hypoxia	0.00178491	4
	response to decreased oxygen levels	0.00178491	
	response to oxygen levels	0.00179384	
	embryo development	0.00211282	
M5	mRNA metabolic process	0.00178491	2

Supplementary Table 3

Primer name	Sequence
ANP32A_Fw	ACTCGGATGCTGAGGGCTAC
ANP32A_Rv	TCTCCACTCACGTCCTCCTC
29S_Fw	GGGTCACCAGCAGCTGTACT
29S_Rv	AAACACTGGCGGCACATATT
VEGF_Fw	TGCAGATTATGCGGATCAAACC
VEGF_Rv	TGCATTCACATTTGTTGTGCTGTAG
TCF1_Fw	CCCCCAACTCTCTCTCTACGA
TCF1_Rv	TGCCTGAGGTCAGGGAGTAG
ATM_Fw	ATCGGCATTCAGATTCCAAA
ATM_Rv	TTTTCTGCCTGGAGGCTTGT
ANP32A_prom1_Fw	ACGGCGATCAGGTTAGTGTG
ANP32A_prom1_Rv	GCCGGCGGAATTCAATCAATAAA
VEGF_prom_Fw	TCACTTTCCTGCTCCCTCCT
VEGF_prom_Rv	GCAATGAAGGGGAAGCTCGA

Supplementary Table 4

Experiment ID	Experiment details
1. DMM OA model, CHIR i.a. injection	* 20-week-old male C57Bl/6J mice (time of sacrifice - induction of model at 8 weeks) * Total sample size: n=15; SHAM Vehicle: n=5, DMM Vehicle: n=5, DMM IOX2: n=5 * Primary outcome: IHC detection of protein expression: Fig3G and FigS1
2. CHIR i.a. injection in C57Bl/6J	* 9-week-old male C57Bl/6J mice * Total sample size: n=6; Vehicle: n=3, CHIR: n=3 * Primary outcome: IHC detection of protein expression: Fig4B and FigS2A
3. 8-week-old *Frzb*$^{-/-}$ mice	* 8-week-old male *Frzb*$^{-/-}$ mice and WT littermates * Total sample size: n=10; WT: n=5, KO: n=5 * Primary outcome: IHC detection of protein expression: Fig4C and FigS2B
4. XAV i.a. injection in C57Bl/6J	* 12-week-old male C57Bl/6J mice * Total sample size: n=6; Vehicle: n=3, XAV: n=3 * Primary outcome: IHC detection of protein expression: Fig4D and FigS2C